Biosensors and Bioelectronics xxx (xxxx) xxx

Contents lists available at ScienceDirect

Biosensors and Bioelectronics

journal homepage: http://www.elsevier.com/locate/bios

Low-background electrochemical biosensor for one-step detection of base excision repair enzyme

Min-hui Zhao [a], Lin Cui [a], Bing Sun [b], Quanbo Wang [c], Chun-yang Zhang [a,*]

[a] College of Chemistry, Chemical Engineering and Materials Science, Collaborative Innovation Center of Functionalized Probes for Chemical Imaging in Universities of Shandong, Key Laboratory of Molecular and Nano Probes, Ministry of Education, Shandong Provincial Key Laboratory of Clean Production of Fine Chemicals, Shandong Normal University, Jinan, 250014, PR China

[b] School of Science, China University of Geosciences (Beijing), Beijing, 100183, China

[c] Laboratory of Immunology for Environment and Health, Shandong Analysis and Test Center, Qilu University of Technology (Shandong Academy of Sciences), Jinan, Shandong, 250014, China

ARTICLE INFO

Keywords:
Electrochemical biosensor
Signal amplification
One-step detection
Mimic enzyme
Host-guest interaction
Low-background signal

ABSTRACT

We develop a low-background electrochemical biosensor for one-step detection of uracil DNA glycosylase (UDG) based on the host-guest interaction and iron-embedded nitrogen-rich carbon nanotube (Fe–N–C) that mimics enzyme-mediated electrocatalysis to achieve signal amplification. In this work, Fe–N–C is initially immobilized on a glassy carbon electrode, followed by the immobilization of β–cyclodextrin (β–CD). We construct the signal probes by assembling the methylene blue (MB)-labeled hairpin DNAs onto the surface of Au nanoparticles (AuNPs) to form the MB-hairpin/AuNP probes. Due to the steric effect of AuNPs and the stem–loop structure of hairpin DNA, MB is prevented from entering the cavity of β-CD on the electrode. In contrast, UDG enables the removal of uracil from the U•A pairs in the stem of hairpin DNA probe to generate apurinic/apyrimidinic (AP) sites, leading to the assembly of MB-hairpin/AuNP probes on the electrode based on host–guest reaction between β-CD and MB. Meanwhile, L-cysteine (RSH) is oxidized by O_2 to disulfide L-cystine (RSSR) and H_2O_2. In the presence of H_2O_2, Fe–N–C catalyzes the oxidation of MB to generate an amplified electrochemical signal. Notably, the Fe–N–C-catalyzed oxidation of MB is mediated by the oxidation of RSH by O_2 instead of external H_2O_2, greatly simplifying the experimental procedures and improving the electrochemical signal. Due to the introduction of host–guest recognition, this electrochemical biosensor displays a low-background signal and high signal-to-noise ratio, enabling the one-step sensitive measurement of UDG with a detection limit of 7.4×10^{-5} U mL^{-1}. Moreover, this biosensor can measure UDG in crude cell extracts and screen the inhibitors, providing a new platform for biomedical research.

1. Introduction

Natural enzymes feature high activity and good specificity with an essential role in the metabolism of organism and various bio-chemical reactions (Gao et al., 2007; Yoon and Mirkin, 2008). However, natural enzymes face great challenges including high cost of preparation, purification and storage, easy denaturation under harsh conditions, and the inhibition of catalytic activity in some complex media (e.g., waste water) (Lin et al., 2014). The requirement of effective and specific enzymes motivates chemists to engineer synthetic enzymes with similar structures and mimic functions to natural enzymes using novel nanotechnologies, consequently generating many functional nanomaterials. Noble metals (e.g., Pd (Ge et al., 2016), and Au (Jv et al., 2010), metal oxides (e.g., MnO_2 (Liu et al., 2017), Fe_3O_4 (Wang et al., 2014), CeO_2 (Naganuma, 2017), carbon-based nanomaterials (Hu et al., 2018), metal complexes (Cui et al., 2015), metal–nitrogen–carbon composites (M-N-C, M = Fe, Co) (Cheng et al., 2019; Jiao et al., 2019), porphyrins (Xu et al., 2013), and polymers (Takagishi and Klotz, 1972) have been extensively explored to mimic the structures and functions of natural enzymes (Wei and Wang, 2013). In comparison with natural enzymes, nanomaterials may serve as the promising candidates for synthetic enzymes due to their distinct advantages of low cost, tunability in catalytic activity, improved stability, robustness under harsh environmental conditions (e.g., methanol, ethanol, and dimethylformamide), and ease of long-term storage and treatment (Lin et al., 2013).

Supramolecular host−guest recognition via noncovalent interaction

* Corresponding author.
E-mail addresses: zpbzcl@126.com (M.-h. Zhao), sunbing@cugb.edu.cn (Q. Wang), cyzhang@sdnu.edu.cn (C.-y. Zhang).

https://doi.org/10.1016/j.bios.2019.111865
Received 19 September 2019; Received in revised form 7 November 2019; Accepted 8 November 2019
Available online 11 November 2019

is a new approach for the assembly of large functional structures (Fan et al., 2011; Jiang et al., 2017). Generally, the host contains a large-volume cavity (e.g., β-cyclodextrins (β-CD)) with outstanding recognition and encapsulation capability towards its guest molecules (Prochowicz et al., 2017; Szente and Szemen, 2013). As the recognition motifs are specific and bioorthogonal, the host–guest interaction has been extensively applied to bioanalysis (Fan et al., 2011; Gao et al., 2015; Jiang et al., 2018; Xie et al., 2015). The Yuan group developed a "signal-on" target-induced ferrocene-labeled peptide cleavage-mediated electrochemical assay for prostate specific antigen detection based on the β-CD−ferrocene recognition (Xie et al., 2015). In their work, the β-CD was adsorbed on carbon materials (e.g., graphene and carbon nanotubes) to ameliorate the dispersion and stability of carbon nanomaterials in aqueous media. Jiang et al. demonstrated an electrochemical biosensor for the monitoring of DNA and miRNA concentrations based on host−guest recognition between the ferrocene-labeled hairpin probe and nitrogen-doped reduced graphene oxide/β-CD polymer nanocomposites (Jiang et al., 2017), but the uncleaved hairpin probes in the paper exhibit a high background signal.

Base excision repair is one of DNA repair mechanisms, in which DNA glycosylase (UDG) plays pivotal roles in maintaining genomic integrity (David et al., 2007). UDG is able to remove uracil lesions from DNA by catalyzing the hydrolysis of N-glycosidic bond between the uracil and the deoxyribose (Schaerer, 2003). As UDG is essential to DNA lesion repair and is associated with both individual and population disease susceptibility, UDG has become a promising biomarker and potential therapeutic target (Thomas et al., 2012). Conventional methods for UDG assay include gel electrophoresis (Dianov, 2003), radioactive assay (Grin et al., 2009), and chromatography (Gackowski et al., 2003), but these methods are usually time- and labor-consuming with the involvement of hazardous radioactive materials (Krokan and Wittwer, 1981) and complicated procedures (Tchou et al., 1991). Alternatively, several new strategies including colorimetric (Zhang et al., 2012) and fluorescent methods (Leung et al., 2013; Zhang et al., 2017) have been developed for UDG assay, but they involve complex preparation procedures for hairpin probes (Zhang et al., 2012) and dye-labeled functional nucleic acid probes (Zhang et al., 2017). Consequently, it is highly desirable to develop simple and sensitive methods for DNA glycosylase assay. Electrochemical biosensors have distinct advantages of low cost, portability and high sensitivity (Xie et al., 2015; Jiang et al., 2017; Thomas et al., 2012).

In this research, we demonstrate the facile and scalable synthesis of iron-embedded nitrogen-rich carbon nanotube (Fe–N–C) by a simple thermal treatment, and further develop a low-background electrochemical biosensor for a one-step detection of UDG involving host-guest interaction. By mimicking enzyme-mediated electrocatalysis, Fe–N–C is used to achieve signal amplification. Due to the abundant catalytically active sites of an iron-embedded nitrogen-rich Fe–N–C, the Fe–N–C possesses good conductivity and it can directly electrocatalyze the reduction of thionines with higher electrocatalytical activity than horseradish peroxidase (HRP) (Cui et al., 2019), significantly amplifying the electrochemical signal. Herein, we design an electrochemical biosensor using a noble metal-free nanoelectrocatalysts with the characteristics of low cost, good stability in alkaline and high ORR performance (Asefa, 2016; Bo et al., 2015; Lv et al., 2017) and host-guest interaction for one-step detection of UDG. We use the L-cysteine (RSH) as the relatively stable catalytic substrate (Youm et al., 2015; Zheng et al., 2016), avoiding the instability and easy decomposition of externally H_2O_2. This electrochemical biosensor exhibits high sensitivity with a detection limit of 7.4×10^{-5} U mL^{-1} and can measure UDG activity in cell extracts.

2. Materials and methods

2.1. Materials and reagents

Dicyandiamide, tris(hydroxymethyl)aminomethane (Tris), gold chloride ($HAuCl_4$), tris(2-carboxyethyl)phosphine hydrochloride (TCEP), 6-mercaptohexanol (MCH), 3,3′,5,5′-tetramethylbenzidine (TMB), bovine serum albumin (BSA) and HRP (EC 1.11.1.7, 261 Units mg^{-1}, powder) were purchased from Sigma-Aldrich. Human alkyladenine DNA glycosylase (hAAG), formamidopyrimidine DNA glycosylase (FPG), uracil glycosylase inhibitor (UGI), UDG, 10 × UDG reaction buffer (200 mM Tris-HCl, 10 mM EDTA, 10 mM DL-Dithiothreitol (DTT), pH 8.0) were obtained from New England Biolabs Inc. (Beverly, MA, U.S.A.). RSH was purchased from J&K Chemical Ltd. Ultrapure water obtained from a Millipore water purification system (≥18 MΩ, Milli-Q, Millipore, U.S.A.) was used in all assays. The synthetic oligonucleotides were purchased from Sangon Biological Engineering Technology & Services Co., Ltd. (Shanghai, China) and purified by using high-performance liquid chromatography. Sequences of the hairpin probe is 5′–HS–***UUU GUC UGU*** **GA**A GGA GGT AGA **TCA CAG ACA AA**-$(CH_2)_6$-MB-3' (The binding regions in hairpin probe are shown in bold, and the cutting bases are highlighted in italic).

2.2. Apparatus

The transmission electron microscopic (TEM) images were obtained by a JEOL JEM 2010 electron microscope (JEOL Ltd., Japan) at 200 kV. Powder X-ray diffraction (XRD) patterns were obtained using a Rigaku D/MAX 2200 PC X-ray diffractometer (X'Pert Pro Super, Philips) with Cu Kα radiation (λ = 0.154178 nm, graphite monochromator, 28 kV and 20 mA), a 2θ range from 10° to 80° at a scanning rate of 10° min^{-1}. Cyclic Voltammetry (CV) and different pulse voltammetry (DPV) were performed on a CHI 660D electrochemical workstation (CHI, Shanghai, China) at room temperature using a conventional three-electrode system with a modified glassy carbon electrode (GCE) as the working electrode, a platinum wire as the auxiliary electrode, and a saturated calomel electrode (Caution: calomel electrode should be handled with great care) as the reference electrode. Electrochemical impedance spectroscopic (EIS) analysis was performed with a Zahner workstation (Zahner, German) in 0.1 M KCl containing 5 mM $[Fe(CN)_6]^{3-}/[Fe(CN)_6]^{4-}$ over a frequency range from 10 kHz to 0.1 Hz using an alternative voltage with a peak-to-peak amplitude of 10 mV. UV–vis absorption spectra were obtained on a Hitachi U-3900 UV–vis spectrophotometer (JEOL Ltd., Japan).

2.3. Synthesis of Fe–N–C

A homogeneous solid mixture of dicyandiamide (12 mmol) and iron (II) chloride hexahydrate ($FeCl_2{\cdot}6H_2O$, 1.68 mmol) was placed in an alumina boat and heated to 500 °C in a tube furnace for 2 h in an argon atmosphere. The temperature in the tube furnace was further raised to 900 °C at a ramp of 10 °C min^{-1} and kept at 900 °C for 2 h in Ar atmosphere to obtain black powder material. After grinding the material to fine powders, the obtained Fe–N–C was kept in a desiccator.

2.4. Measurement of Fe–N–C peroxidase activity

In this work, 10 μL of 100 μg mL^{-1} Fe–N–C, 10 μL of a 200 mM acetate buffer (pH 4.0) and 60 μL of ultrapure water were mixed and incubated for 30 min under mild vortexing. Subsequently, 10 μL of TMB in dimethyl sulfoxide (DMSO) solution (5 mM) and 10 μL of 50 mM hydrogen peroxide (H_2O_2) were injected into the mixture to initiate the oxidation reaction for 5 min at room temperature.

2.5. Preparation of AuNPs and the MB-hairpin/AuNP probes

For the synthesis of AuNPs, 100 mL of 0.01% $HAuCl_4$ solution was boiled with vigorous stirring, followed by quick addition of 2.5 mL of 1% trisodium citrate solution (Ambrosi et al., 2007). The mixture solution was kept boiling for 30 min, followed by cooling down to room temperature. When the AuNPs were formed, the solution turned deep red, followed by stirring and cooling down. The obtained AuNPs were stored in a brown glass bottle at 4 °C until further use.

The MB-hairpin probes were diluted to 10 μM in a buffer (1.5 mM $MgCl_2$, 10 mM Tris-HCl, pH 8.0), and then incubated at 95 °C for 5 min, followed by slowly cooling down to room temperature over 30 min to fold into a hairpin structure. Then the thiolated MB-hairpin probes (10 μM) were activated by 1 mM TCEP for 1 h to reduce the disulfide-bonded oligonucleotides. AuNPs were mixed with the MB-hairpin probes for 16 h, and the resulting solution was centrifugated at 12 000 rpm for 20 min to remove the excess oligonucleotides. The wine-red MB-hairpin/AuNP precipitate was washed with 0.1 M PBS and redispersed in 0.1 M PBS. The resulting probe solution was stored in the refrigerator until use. The MB-hairpin@AuNPs were characterized by UV spectrophotometry (JEOL Ltd., Japan).

2.6. Preparation of electrochemical biosensing platform

The electrochemical biosensor was constructed on a GCE electrode. Prior to the modification, the GCE electrode was sequentially polished using 1.0, 0.3, and 0.05 μm α-Al_2O_3 slurry, followed by successive sonication with distilled water and ethanol for 3 min. The 10 μL of Fe–N–C solution (2 mg mL^{-1}) was applied to the GCE surface to obtain the Fe–N–C/GCE. After drying at room temperature, 10 μL of β-CD (2 mM) was applied to the Fe–N–C/GCE to obtain the β-CD/Fe–N–C/GCE.

2.7. Electrochemical detection of UDG and inhibition assay

The 5 μL of MB-hairpin/AuNPs probes were added to the reaction solution (10 μL) containing various-concentration UDG, and 1 μL of 10× UDG reaction buffer. The 10 μL of MB-hairpin/AuNPs probes were delivered on the β-CD/Fe–N–C/GCE and incubated at 37 °C for 80 min. The electrode was stored at 4 °C after thoroughly rinsing and drying in nitrogen. In addition, UDG inhibition assay was investigated with UGI as the model inhibitor. Similar procedures for UDG assay were employed for UDG inhibition assay except that the inhibitor UGI at various concentrations was premixed with the reaction buffer containing 1 U mL^{-1} UDG.

2.8. Cell culture

HeLa cells were cultured in Dulbecco's modified Eagle's medium (DMEM; Gibco, U.S.A.) supplemented with 10% fetal bovine serum (FBS, Gibco, U.S.A.) and 1% penicillin-streptomycin (Gibco, U.S.A.) in 5% CO_2 incubator at 37 °C. HeLa cells were collected with trypsinization in the exponential phase of growth, washed twice with ice-cold PBS (pH 7.4, Gibco, U.S.A.), and centrifuged at 1000 rpm for 5 min. Then the cells were suspended in 100 μL of lysis buffer (10 mM Tris-HCl, pH 8.0, 150 mM NaCl, 1% NP-40, 0.25 mM sodium deoxycholate, 1.0% glycerol, and 0.1 mM 4-(2-aminoethyl) benzenesulfonylfluoride hydrochloride), and incubated on ice for 30 min, followed by centrifuging at 12,000 g for 20 min at 4 °C. The supernatant was transferred into a fresh tube and stored at −80 °C.

3. Results and discussion

3.1. Principle of electrochemical biosensor for UDG assay

The principle of electrochemical biosensor for UDG assay is shown in Scheme 1. The Fe–N–C solution was applied onto the GCE surface to obtain the Fe–N–C/GCE. After drying at room temperature, β-CD was assembled on the Fe–N–C/GCE to acquire the β-CD/Fe–N–C/GCE. The DNA substrate is designed as a hairpin structure with a stem and a loop. The stem contains two complementary strands including a MB-labeled 3′-end stem and a thiol-labeled 5′-end stem with four uracil bases. After the 5′ end of the probe is conjugated with AuNP, the probe is in a stem-loop structure with the MB label at the 3′ end being close to the AuNP surface, and consequently MB cannot be captured by the β-CD/Fe–N–C/GCE, leading to a low background current due to the steric effect of AuNPs and the stem-loop structure of hairpin DNA. The presence of UDG can promote the removal of six uracil bases from U·A pairs in the stem of hairpin DNA, generating apurinic/apyrimidinic sites and leading to a straight single-stranded DNA with MB at the 3′ end. MB can be recognized by β-CD through host−guest interaction and assembles on the electrode, resulting in a significantly enhanced peak current of MB compared with that in the absence of target UDG. Meanwhile, L-cysteine with thiol structure (RSH) is converted to RSSR by the dissolved O_2 in the solution, accompanied by the release of H_2O_2. With the assistance of H_2O_2, Fe–N–C catalyzes the oxidation of MB to MB_{ox} (He et al., 2018; Zhang et al., 2013a, b), which is reduced on the electrode to generate an amplified electrochemical signal (Zheng et al., 2016). Due to the involvement of the Fe–N–C mimic enzyme with high electrocatalysis efficiency, the more stable catalytic substrate RSH, and the supramolecular host-guest interaction strategy, the proposed biosensor possesses the advantages of extremely low background and high signal amplification, making it suitable for sensitive detection of UDG activity.

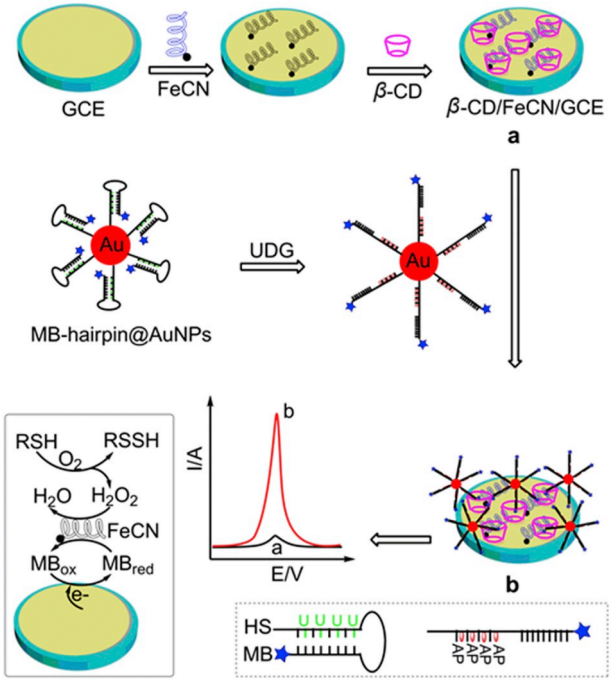

Scheme 1. Schematic illustration of electrochemical biosensor for one-step detection of UDG with the host–guest interaction and Fe–N–C mimic enzyme-mediated electrocatalytic amplification.

3.2. Characterization of different nanomaterials

We used XRD to investigate the crystalline structure of Fe–N–C (Fig. 1A). The peak at 26.2° represents the characteristic diffraction of carbon (002) plane after comparing this to the structural feature of carbon nanotubes in Fan et al.'s work (2015) involving Fe_3C nanocrystals encased in graphene nanoribbons. The peaks in the range of 40–50° can be indexed to the diffraction of Fe_3C structure (Yang et al., 2015) (JCPDF No. 89–2867), indicating the formation of Fe–N–C after

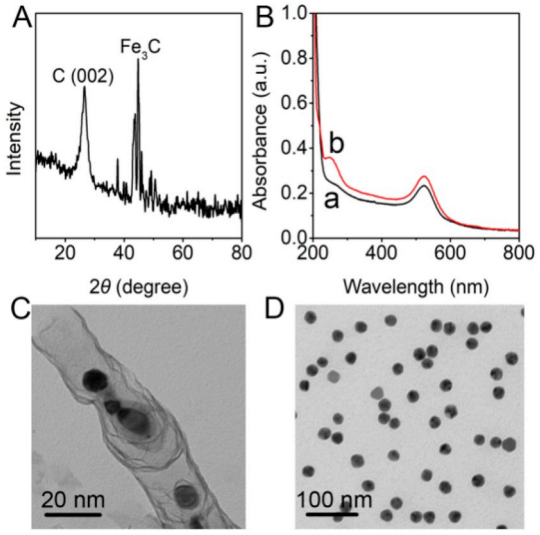

Fig. 1. (A) XRD pattern of Fe–N–C. (B) UV–vis spectra of AuNPs (black curve), and MB-hairpin/AuNPs (red curve). (C–D) TEM images of Fe–N–C (C) and AuNPs (D). (For interpretation of the references to color in this figure legend, the reader is referred to the Web version of this article.)

the thermal polycondensation and carbonization (Xiang et al., 2014). We used UV–vis absorption spectroscopy to characterize the MB-hairpin/AuNPs conjugates (Fig. 1B). An adsorption peak at 518 nm is observed for 10-nm AuNPs (Fig. 1B, black curve). After the modification of AuNPs by hairpin probes, a slight shift of the surface plasmon resonance peak from 518 to 522 nm is observed due to the increase of AuNP diameter induced by the conjugation of hairpin DNAs to the AuNPs (Fig. 1B, red curve) (Xu and Craig, 2007). Notably, a new absorption peak emerges at 260 nm, which is the characteristic absorption peak of the double bond of DNA bases that was reported by Zhang et al. (2016) in their work involving gold nanoparticle–DNA complexes, indicating the formation of MB-hairpin/AuNPs conjugates (Zhang et al., 2016). Fig. 1C shows a typical transmission electron micrograph image of the synthesized Fe–N–C with a few Fe nanoparticles being inserted in the CN nanotubes. In addition, the morphology of AuNPs was investigated with TEM. It exhibits a uniform shape with an average diameter of 13 nm (Fig. 1D).

3.3. Assay feasibility

EIS is employed to characterize the electrochemical behaviors of the modified electrode at different stages in 5 mM $[Fe(CN)_6]^{3-}$ and 5 mM $[Fe(CN)_6]^{4-}$ solution. Fig. 2A shows the impedance spectra of the modified electrodes formed in different construction steps and their corresponding equivalent circuit. The R_s, Z_w, R_{ct}, and CPE represent the Ohmic resistance of the electrolyte, Warburg impedance, charge-transfer resistance, and constant phase angle element, respectively, and R_{ct} is fitted from Nyquist diagram using "auto lab" software. When Fe–N–C is coated onto the GCE, the R_{ct} is decreased to 22 Ω (Fig. 2A, **curve b**) compared to that of bare GCE (750 Ω) (Fig. 2A, **curve a**) due to the good conductivity of Fe–N–C. After attaching β-CD on the Fe–N–C/GCE, the R_{ct} is further increased to 50 Ω (Fig. 2A, **curve c**). However, after MB-hairpin/AuNPs assembly has reacted with 1 U mL^{-1} UDG, R_{ct} is increased to 560 Ω (Fig. 2A, **curve d**) due to the electrostatic repulsion of $[Fe(CN)_6]^{3-/4-}$ by the negatively charged phosphate backbones of hairpin probes.

The feasibility of the proposed biosensor is explored with different modified electrodes based on their DPV responses towards 1 U mL^{-1} UDG. As shown in Fig. 2B, no detectable electrochemical signal is detected in the absence of UDG (Fig. 2B, **curve a**), but a DPV peak of 5.05 μA, corresponding to the reduction of MB, is observed in the

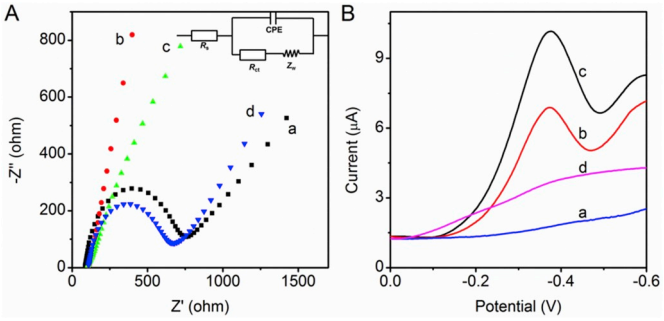

Fig. 2. (A) Nyquist plots of EIS of the modified GCE electrode in 5 mM $[Fe(CN)_6]^{3-}$ and 5 mM $[Fe(CN)_6]^{4-}$: (a) the GCE, (b) the Fe–N–C/GCE, (c) the β-CD/Fe–N–C/GCE, and (d) the MB-hairpin/AuNPs + 1 U mL^{-1} UDG + the β-CD/Fe–N–C/GCE; Inset: the electrical equivalent circuit applied to fit the impedance data; R_s, Z_w, R_{ct}, and CPE represent the Ohmic resistance of the electrolyte, Warburg impedance, charge-transfer resistance, and constant phase angle element, respectively. (B) DPV curves of the β-CD/Fe–N–C/GCE (a, b, c) and the Fe–N–C/GCE (d) incubated with the MB-hairpin/AuNPs in the absence (a) and (b, c, d) presence of 1 U mL^{-1} UDG in 0.1 M PBS (pH 7.4) without (a, b) and with (c, d) 10 mM L-cysteine.

presence of UDG (Fig. 2B, **curve b**). Notably, the amplification of electrochemical signal (Fig. 2B, **curve b**) is initially derived from Fe–N–C which enables the electrocatalytic reduction of MBs by the dissolved O_2 without addition of H_2O_2 (Cui et al., 2019). After the addition of L-cysteine in the electrolyte, the DPV peak current of MB is further increased to 8.33 μA (Fig. 2B, **curve c**). This can be explained by the fact that L-cysteine with thiol structure is oxidized by O_2 to release H_2O_2, promoting the Fe–N–C-catalyzed oxidation of electron mediator MB to generate an amplified electrochemical signal. In contrast, in the absence of β-CD, the electrochemical signal is decreased to 1.85 μA even in the presence of UDG (Fig. 2B, **curve d**), because MB cannot be assembled on the electrode without β-CD-mediated host-guest interaction.

3.4. Optimization of experimental conditions

To achieve the best assay performance, we optimized the experimental conditions including the concentrations of Fe–N–C and β-CD as well as the incubation time for one-step detection of UDG with the biosensor (Fig. S4). As shown in Fig. S4A, the electrochemical DPV response is enhanced by 4.2 times with increasing concentration of Fe–N–C from 0.5 to 2 mg mL^{-1}, but it decreases by 2.1 times when the concentration exceeds 2 mg mL^{-1} as a high-concentration Fe–N–C may induce the detachment of Fe–N–C from the electrode. Thus, 2 mg mL^{-1} Fe–N–C is used in the subsequent experiments. We further investigated the effect of β-CD concentration upon the assay performance (Fig. S4B). The DPV response enhances by 7.3 times with the increase of β-CD concentration from 0.5 to 2 mM, but it decreases by 3.2 times beyond the concentration of 2 mM due to the saturation of the host-guest interaction and the hindering of electron transfer induced by high-concentration non-conductive β-CD. Thus, 2 mM β-CD is used in the subsequent research. In addition, we optimized the incubation time for one-step detection of UDG with the biosensor (Fig. S4C). The current response enhances by 3.1 times with the incubation time from 40 to 80 min, and then levels off at 99.3% beyond 80 min. Thus, 80 min is selected as the optimal incubation time in the subsequent research.

3.5. Sensitivity and specificity of UDG assay

Under the optimized experimental conditions, we measured the DPV current in response to different concentrations of UDG in 0.1 M PBS (pH 7.4) containing 10 mM L-cysteine (Fig. 3A). The DPV peak current is observed to increase with UDG concentration, and exhibits a linear relationship between the DPV peak current and the UDG concentration

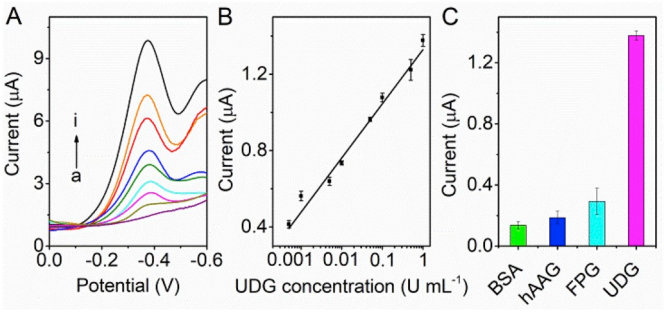

Fig. 3. (A) DPV curves in response to different concentrations (from a to i: 0, 0.0005, 0.001, 0.005, 0.01, 0.05, 0.1, 0.5, 1 U mL^{-1}) of target UDG in 0.1 M PBS (pH 7.4) containing 10 mM L-cysteine. (B) The calibration curve for UDG assay. (C) Specificity of the electrochemical biosensor towards target UDG (1 U mL^{-1}), BSA (0.01 mg mL^{-1}), hAAG (1 U mL^{-1}), and FPG (1 U mL^{-1}). Error bars show the standard deviation of three experiments.

in the range from 0.0005 to 1 U mL^{-1} (Fig. 3B). The regression equation is $I = 1.3 + 0.28 \log_{10} C$ ($R^2 = 0.977$, N = 8), where I is the current intensity and C is the concentration of UDG (U mL^{-1}), respectively. The detection limit of this electrochemical biosensor is estimated to be 7.4×10^{-5} U mL^{-1} by evaluating the average value of the control plus 3 times standard deviation. Notably, this biosensor exhibits a sensitivity of 0.28 μA for every 10-fold change of UDG concentration, which is superior to most of existing assays (Table S1), including at least 27-fold higher than that of fluorescent assay (Jing et al., 2014; Zhang et al., 2012, 2017), 270-fold higher than that of the colorimetric assays (Liu et al., 2014), 107-fold higher than that of electrochemical assays (Jiao et al., 2016; Liu et al., 2013; Zhang et al., 2013a, b). The improved sensitivity can be attributed to three factors: (1) the supramolecular host−guest interaction between MB and β-CD results in an extremely low background due to the steric effect of AuNPs and the stem–loop structure of hairpin DNAs; (2) the mimic peroxidase Fe–N–C exhibits excellent electrocatalytic activity and good stability in wide ranges of pH and temperature; (3) L-cysteine is converted to L-cystine (RSSR) by O_2, accompanied by the release of H_2O_2 which promotes the Fe–N–C-catalyzed oxidation of MB to generate an amplified electrochemical signal. To evaluate the detection specificity, we used nonspecific bovine serum albumin (BSA), human alkyladenine DNA glycosylase (hAAG), formamidopyrimidine-DNA glycosylase (FPG) as the negative controls. BSA cannot recognize and excise uracil from DNA substrate. The hAAG can excise the alkylated adenine to generate an apurinic site (Wu et al., 2013), and FPG can excise 4,6-diamino-5-formamidopyrimidine (FapyAde), 8-hydroxyguanine (8-OH-Gua), and 2,6-diamino-4-hydroxy-5-formamidopyrimidine (FapyGua) (Boiteux et al., 1992), but they cannot cleave the DNA substrate used in this research. As shown in Fig. 3C, a high current signal is detected in response to 1 U mL^{-1} UDG, but the percentage current value of 9.9%, 13.5% and 21.2% is observed in response to 0.01 mg mL^{-1} BSA, 1 U mL^{-1} hAAG, and 1 U mL^{-1} FPG, respectively, compared with 1 U mL^{-1} UDG. These results demonstrate the good specificity of the proposed biosensor towards UDG.

3.6. Repeatability, stability and reproducibility of the electrochemical biosensor

The repeatability of the proposed electrochemical biosensor was investigated through 6 successive assays in the presence of 1 U mL^{-1} UDG. The relative standard deviation (RSD) is 1.6%, suggesting the good repeatability of the proposed electrochemical biosensor. Moreover, after the test, the electrodes were polished and remodified. Under the identical conditions, a current signal change of 5.8% is obtained, demonstrating the good stability and regeneration capability of the proposed electrochemical biosensor. We further examined the interassay precision of the proposed biosensor. The RSD for six parallel measurements with six biosensors fabricated with the same process is 1.9%, indicating the good reproducibility of this biosensor.

3.7. UDG inhibition assay

To demonstrate the feasibility of the proposed electrochemical biosensor for UDG inhibition assay, we employed uracil glycosylase inhibitor (UGI) as the model inhibitor. As shown in Fig. 4, the relative activity of UDG decreases monotonically with increasing concentration of UGI in a dose-dependent manner. This is because UGI can bind with UDG to form a tight and physiologically irreversible complex in a 1:1 concentration-based stoichiometry (Kaushal et al., 2008). The relative activity (RA) of UDG is evaluated according to RA (%) = (N_i - N_0) / (N_t - N_0) × 100 , where N_o, N_t, and N_i represent the peak current in the absence of UDG, in the presence of 1 U mL^{-1} UDG, and in the presence of 1 U mL^{-1} UDG and 1 U mL^{-1} UGI, respectively. This result demonstrates that the proposed electrochemical biosensor can be potentially used to screen the UDG inhibitors.

3.8. Cellular UDG assay

The accurate detection of cellular UDG activity is essential to biomedical research and clinical diagnosis. To demonstrate the capability of the proposed electrochemical biosensor for the analysis of real-life complex biological samples, we used HeLa cells as the model for the detection of cellular UDG activity. As shown in Fig. 5, the peak current exhibits a linear correlation with the logarithm of HeLa cell number in the range from 5 to 10 000 cells. The regression equation is $I = 0.76 \log_{10} N$ - 0.4 with a R^2 of 0.991, where I is the current intensity and N is the number of HeLa cells, respectively. The detection limit of the proposed electrochemical biosensor is calculated to be 5 cells by evaluating the average value of the control plus 3 times standard deviation. This result clearly demonstrates that the proposed electrochemical biosensor can be used to quantitatively detect cellular UDG activity, holding great potential for further applications in clinical diagnosis.

4. Conclusions

In summary, we have developed a new electrochemical biosensor for one-step detection of UDG with host–guest interaction and mimic enzyme-mediated electrocatalysis signal amplification. The target UDG enables the removal of uracil from U·A pairs in the stem of hairpin DNA probe and generates apurinic/apyrimidinic sites, resulting in the assembly of MB-hairpin/AuNPs probes onto the electrode based on the host–guest reaction between β-CD and MB. L-cysteine with thiol structure in electrolyte is oxidized by O_2 to disulfide L-cystine and H_2O_2, which accelerates the Fe–N–C-catalyzed oxidation of MB to generate an amplified electrochemical signal. The proposed electrochemical

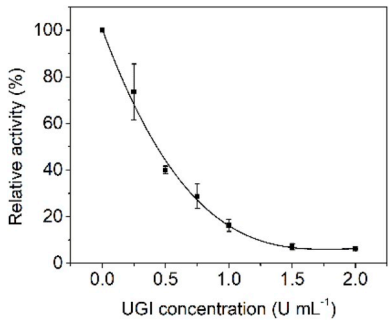

Fig. 4. Variance of the RA of UDG in response to different concentrations of UGI. The concentration of UDG is 1 U mL^{-1}. Error bars show the standard deviation of three experiments.

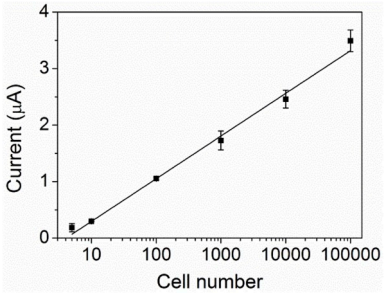

Fig. 5. Linear relationship between the peak current and the logarithm of HeLa cell number. Error bars represent the standard deviations from three replicates.

biosensor has significant advantages of (1) the low background signal resulting from the supramolecular host−guest interaction and the steric effect of AuNPs and the stem–loop structure of hairpin DNA, (2) an amplified electrochemical signal induced by Fe–N–C-catalyzed oxidation of MB, (3) the significant signal enhancement resulting from the assembly of multiple MB-hairpin/AuNP conjugates which carry abundant MBs onto the electrode, (4) the Fe–N–C-catalyzed oxidation of MB is mediated by the oxidation of the more stable catalytic substrate RSH by O_2 instead of external H_2O_2, greatly simplifying the experimental procedures; (5) the proposed electrochemical biosensor can be used for one-step detection of UDG; (6) in comparison with the reported methods (Table S1), the proposed electrochemical biosensor exhibits high sensitivity with a detection limit of as low as 7.4×10^{-5} U mL^{-1}. Moreover, this electrochemical biosensor can be applied for the screening of UDG inhibitors, holding great potential in biomedical research and clinical diagnosis.

Credit author statement

All authors conceived the work and wrote the manuscript. All authors reviewed and approved the manuscript.

Declaration of competing interest

The authors declare that they have no known competing financial interests or personal relationships that could have appeared to influence the work reported in this paper.

CRediT authorship contribution statement

Min-hui Zhao: Conceptualization, Writing - original draft, Writing - review & editing. **Lin Cui:** Conceptualization, Writing - original draft, Writing - review & editing. **Bing Sun:** Writing - original draft, Writing - review & editing. **Quanbo Wang:** Writing - original draft, Writing - review & editing. **Chun-yang Zhang:** Conceptualization, Writing - original draft, Writing - review & editing.

Acknowledgments

This work was supported by the National Natural Science Foundation of China (Grant Nos. 21527811, 21735003, 21605095, 21974080, 21605096, and 21802128), Youth Science Funds of Shandong Academy of Sciences (Grant No. 2018QN001) and the Award for Team Leader Program of Taishan Scholars of Shandong Province, China.

Appendix A. Supplementary data

Supplementary data to this article can be found online at https://doi.org/10.1016/j.bios.2019.111865.

References

Ambrosi, A., Castañeda, M.T., Killard, A.J., Smyth, M.R., Alegret, S., Merkoçi, A., 2007. Anal. Chem. 79, 5232–5240.
Asefa, Tewodros, 2016. Acc. Chem. Res. 49, 1873–1883.
Bo, X.J., Li, M., Han, C., Zhang, Y.F., Nsabimanaa, A., Guo, L.P., 2015. J. Mater. Chem. 3, 1058–1067.
Boiteux, S., Gajewski, E., Laval, J., Dizdaroglu, M., 1992. Biochemistry 31, 106–110.
Cheng, N., Li, J.-C., Liu, D., Lin, Y.H., Du, D., 2019. Small. https://doi.org/10.1002/smll.201901485.
Cui, L., Wang, M., Sun, B., Ai, S., Wang, S., Zhang, C.-y., 2019. Chem. Commun. 55, 1172–1175.
Cui, L., Wu, J., Li, J., Ju, H., 2015. Anal. Chem. 87, 10635–10641.
David, S.S., O'Shea, V.L., Kundu, S., 2007. Nature 447, 941–950.
Dianov, G.L., 2003. Toxicology 193, 35–41.
Fan, H., Xu, Y., Chang, Z., Xing, R., Wang, Q., He, P., Fang, Y., 2011. Biosens. Bioelectron. 26, 2655–2659.
Fan, X., Peng, Z., Ye, R., Zhou, H., Guo, X., 2015. ACS Nano 9, 7407–7418.
Gao, J., Guo, Z., Su, F., Gao, L., Pang, X., Cao, W., Du, B., Wei, Q., 2015. Biosens. Bioelectron. 63, 465–471.
Gao, L., Zhuang, J., Nie, L., Zhang, J., Zhang, Y., Gu, N., Wang, T., Feng, J., Yang, D., Perrett, S., 2007. Nat. Nanotechnol. 2, 577.
Ge, C., Fang, G., Shen, X., Chong, Y., Wamer, W.G., Gao, X., Chai, Z., Chen, C., Yin, J.-J., 2016. ACS Nano 10, 10436–10445.
Grin, I.R., Konorovsky, P.G., Nevinsky, G.A., Zharkov, D.O., 2009. Biochemistry 74, 1253–1259.
Gackowski, D., Speina, E., Zielinska, M., Kowalewski, J., Rozalski, R., Siomek, A., Paciorek, T., Tudek, B., Olinski, R., 2003. Cancer Res. 63, 4899–4902.
He, J.C., Zhang, Y., Zhang, X.D., Huang, Y.M., 2018. Sci. Rep. 8, 5159.
Hu, Y., Gao, X.J., Zhu, Y., Muhammad, F., Tan, S., Cao, W., Lin, S., Jin, Z., Gao, X., Wei, H., 2018. Chem. Mater. 30 (18), 6431–6439.
Jiang, J., Lin, X., Diao, G., 2017. ACS Appl. Mater. Interfaces 9, 36688–36694.
Jiang, J., Lin, X., Dong, D., Diao, G., 2018. Biosens. Bioelectron. 114, 37–43.
Jiao, F., Qian, P., Qin, Y., Xia, Y., Deng, C., Nie, Z., 2016. Talanta 147, 98–102.
Jiao, L., Xu, W.Q., Yan, H.Y., Wu, Y., Liu, C.R., Du, D., Lin, Y.H., Zhu, C.Z., 2019. Anal. Chem. 91, 11994–11999.
Jing, T., Panshu, S., Yusuke, S., Seiichi, N., Norio, T., Aijun, T., Yu, X., 2014. Chem. Commun. 51, 929–932.
Jv, Y., Li, B., Cao, R., 2010. Chem. Commun. 46, 8017–8019.
Kaushal, P.S., Talawar, R.K., Krishna, P., Varshney, U., Vijayan, M., 2008. Acta Crystallogr. 64, 551–560.
Krokan, H., Wittwer, C.U., 1981. Nucleic Acids Res. 9, 2599–2613.
Leung, C.H., Zhong, H.J., He, H.Z., Lu, L., Chan, D.S.H., Ma, D.L., 2013. Chem. Sci. 4, 3781–3795.
Lin, Y., Ren, J., Qu, X., 2014. Acc. Chem. Res. 47, 1097–1105.
Lin, Y., Zhao, A., Tao, Y., Ren, J., Qu, X., 2013. J. Am. Chem. Soc. 135, 4207–4210.
Liu, J., Meng, L., Fei, Z., Dyson, P.J., Jing, X., Liu, X., 2017. Biosens. Bioelectron. 90, 69–74.
Liu, X., Chen, M., Hou, T., Wang, X., Liu, S., Feng, L., 2013. Electrochim. Acta 113, 514–518.
Liu, X., Chen, M., Hou, T., Wang, X., Liu, S., Feng, L.I., 2014. Biosens. Bioelectron. 54, 598–602.
Lv, Q., Si, W.Y., Yang, Z., Wang, N., Tu, Z.Y., Yi, Y.P., Huang, C.S., Jiang, L., Zhang, M.J., He, J.J., Long, Y.Z., 2017. ACS Appl. Mater. Interfaces 9, 29744–29752.
Naganuma, T., 2017. Nano Res. 10, 199–217.
Prochowicz, D., Kornowicz, A., Lewinski, J., 2017. Chem. Rev. 117, 13461–13501.
Schaerer, O.D., 2003. ChemInform 34, 2946–2974.
Szente, L., Szeman, J., 2013. Anal. Chem. 85, 8024–8030.
Takagishi, T., Klotz, I.M., 1972. Biopolymers 11, 483–491.
Tchou, J., Kasai, H., Shibutani, S., Chung, M.H., Laval, J., Grollman, A.P., Nishimura, S., 1991. Proc. Natl. Acad. Sci. U. S. A. 88, 4690–4694.
Thomas, H., Eva, P., Cecilia, L., Ben, H., Sharma, R.A., 2012. Toxicol. Lett. 211. S9-S9.
Wang, H., Li, S., Si, Y., Sun, Z., Li, S., Lin, Y., 2014. J. Mater. Chem. B. 2, 4442–4448.
Wei, H., Wang, E., 2013. Chem. Soc. Rev. 42, 6060–6093.
Wu, Y., Zhang, B., Guo, L.H., 2013. Anal. Chem. 85, 6908–6914.
Xiang, J., Li, J., Zhang, X., Ye, Q., Xu, J., Shen, X., 2014. J. Mater. Chem. 2, 16905–16914.
Xu, J., Craig, S.L., 2007. Langmuir 23, 2015–2020.
Xu, J., Wu, J., Zong, C., Ju, H., Yan, F., 2013. Anal. Chem. 85, 3374–3379.
Xie, S., Zhang, J., Yuan, Y., Chai, Y., Yuan, R., 2015. Chem. Commun. 51, 3387–3390.
Yang, W., Liu, X., Yue, X., Jia, J., Guo, S., 2015. J. Am. Chem. Soc. 137, 1436–1439.
Yoon, H.J., Mirkin, C.A., 2008. J. Am. Chem. Soc. 130, 11590–11591.
Youm, Y., Dryer, R.F., Thambyrajah, K., Flatt, A.E., Sprague, B.L., 2015. Biosens. Bioelectron. 66, 585–589.
Zhang, H., Dong, H., Yang, G., Chen, H., Cai, C., 2016. Anal. Chem. 88, 11108–11114.
Zhang, H., Zhang, L., Jiang, J., Yu, R., 2013. Anal. Sci. 29, 193–198.
Zhang, L., Zhao, J., Jiang, J., Yu, R., 2012. Chem. Commun. 48, 8820–8822.
Zhang, Y., Li, C.C., Tang, B., Zhang, C.Y., 2017. Anal. Chem. 89, 7684–7692.
Zhang, Z., Hao, J.H., Yang, W.S., Lu, B.P., Ke, X., Zhang, B.L., Tang, J.L., 2013. ACS Appl. Mater. Interfaces 5, 3809–3815.
Zheng, Y., Yuan, Y., Chai, Y., Yuan, R., 2016. Biosens. Bioelectron. 79, 86–91.